CrossMark

TECHNICAL PAPER

Numerical and experimental study of the filling stage of roll-to-roll UV embossing process with micro features

**X. Song · X. C. Shan · S. L. Chow ·
X. Y. Deng · W. S. Teo**

Abstract Roll-to-roll (R2R) UV embossing is a promising low cost and high throughput process that leverages on rapid photo-curing to achieve high embossing speeds for manufacturing large area functional films. There are many potential commercial applications of this process such as flexible displays and functional optical films. However, productivity improvement was hindered by the low web speed at which the system can run without losing the feature fidelity. The current work aims to study the filling-stage of the R2R UV embossing process for s via numerical simulation and experimental validation, in order to better understand the process and identify the limiting factor for productivity improvement. Coupled Eulerian–Lagrangian algorithm was employed in the simulation to consider both deformation of the solid backing film and flow of the liquid UV resin. Their interaction is deemed to influence the mold filling distance. Model predicts that for the web speed of 3 and 30 m/min, the mold filling distance increases fractionally from 2.4 to 2.8 mm, indicating that the filling stage plays a minor role in the feature fidelity control if air entrapment is not considered. Experiments with the micro feature embosser further validate the simulation in a way that to point out it is the air entrapment which causes the incomplete filling. Some basic design rules of the micro features are also provided.

1 Introduction

Micro embossing, including micro hot embossing (Becker and Heim 2000; He et al. 2007; Li et al. 2008) and ultraviolet

(UV) embossing (Lee 2007; Guo 2004), was originally implemented as planar embossing. In which, a planar mold (template) with micro structures of micrometer scale is pressed onto a material for micro replication. Planar embossing is regarded as a high-resolution and low-cost process, and it has been widely used for fabricating functional structures such as those used in micro fluidic devices and optical components. However, planar embossing process has its limitations. One is the small embossing area due to the size of mold and substrate. Increasing the size of a mold can increase embossing area, but this will increase the difficulty in demolding. Another limitation is the low process throughput, since the planar embossing is normally conducted piecewise (Schift 2008). Numerical simulation study of planar embossing process has been widely explored over last decade, and notable examples include those of Worgull and Heckele's work (Worgull and Heckele 2004; Worgull et al. 2006) on hot embossing process simulation for micro- and nano-component fabrication. Thermo-viscoelastic behavior material model of amorphous thermoplastics was considered for the entire hot embossing process, including molding, curing and demolding. However, for UV embossing, as the UV curable materials are thermoset, the curing kinetics and material behaviours are quite different from those of thermoplastics and no single constitutive model can be used for the entire process. Generally speaking, the UV curable materials are treated as liquid in the molding stage and solid in the demolding stage separately (Yeo et al. 2009) in the simulation (hence different constitutive equations and simulation methods).

In a typical roll-to-roll (R2R) embossing process (Makela 2008), the molding, curing and demolding processes all happen around an embossing roller (Fig. 1, UV embossing module). The substrate, which is usually a flexible film, is continuously fed into the embossing roller for

X. Song (✉) · X. C. Shan · S. L. Chow · X. Y. Deng · W. S. Teo
Singapore Institute of Manufacturing Technology,
A*STAR, Singapore 638075, Singapore
e-mail: xsong@SIMTech.a-star.edu.sg

micro-structuring. Hence, it is a continuous process which provides large area manufacturing capability with low cost and high throughput (Makela 2008; Yeo et al. 2010; Shan et al. 2009; Ahn and Guo 2009). Furthermore, R2R ultraviolet (UV) embossing has advantages over R2R hot embossing in terms of low process temperature, low embossing pressure and high process speed (Nezuka et al. 2008; Ahn and Guo 2008). However, only R2R hot embossing process has been studied so far through numerical simulation (Sahli et al. 2010; Sahli et al. 2009), R2R UV embossing is rarely explored by the research community due to its complex setup (roller template and flexible substrate introduces large rotation and deformation both in the film and resin) and Fluid and Structure Interaction (FSI) nature. The work presented here is the first attempt to tackle this problem though numerical simulation using newly available CEL algorithm. The filling stage of the UV embossing process will be the focus of the current work. An experimental study of the embosser mold filling is also carried out to complement the observation from the simulation.

2 Numerical and experimental methods

2.1 R2R UV embossing system setup

An in-house-developed R2R UV embossing system has been employed in the current study (as illustrated in Fig. 1) (Shan et al. 2011). It consists of four basic modules:

1. Unwinding module: it is used as a film supplier module to handle original polymer films
2. Coating module: it consists of a slot die coater, which has a coating width of 250 mm and a slot opening of 100 µm in width. The slot die coater is used for depositing UV curable resin on polymer films
3. Embossing module: it consists of an embossing roller with patterns and used for embossing micro structures via replication and UV exposure from bottom
4. Rewinding module: It consists of a motorized reel and is used for receiving the embossed film with embossed microstructures on its surface

In the current UV embossing system, the embossing roller is 500 mm long in axial direction with a diameter of 160 mm. Large format mold for R2R UV embossing is manufactured machining micro features on a 600 µm brass sheet, which is then wrapped onto an embossing roller and welded together (Fig. 2a). Mould release (Nano mould release™) was applied onto the mould before the embossing experiments and cure at 80 °C for 1 h. On the mould, surface features of discrete pillars (Fig. 2b, Cluster 2) and channels along the roller axial direction (horizontal, Fig. 2b, Cluster 1) and against the roller axial direction (vertical, Fig. 2b, Cluster 3) were created, with feature width of 300 µm and feature height of 210 µm (Aspect Ratio = 0.7), 300 µm (AR = 1) and 450 µm (AR = 1.5), and taping angle of 1°, 2°, 5°, 10° and 35° (Fig. 2c). One example of the 3D optical microscope measurement of the
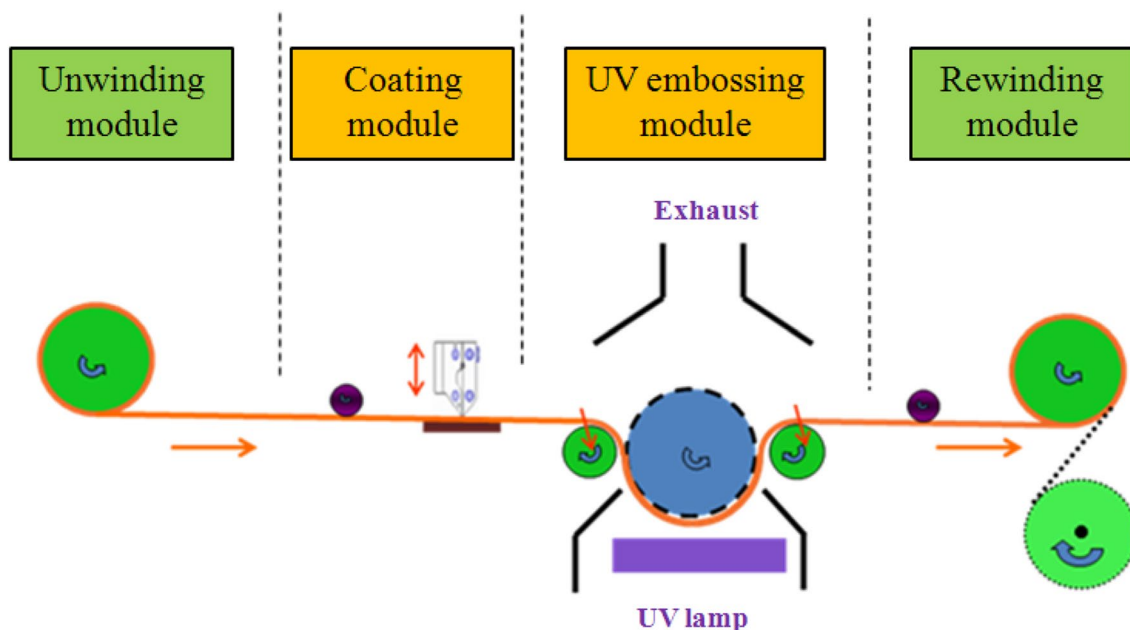
Fig. 1 Schematic diagram of the developed R2R UV embossing system. The embossing system consists of four modules, which are unwinding module, coating module, UV embossing module and rewinding module
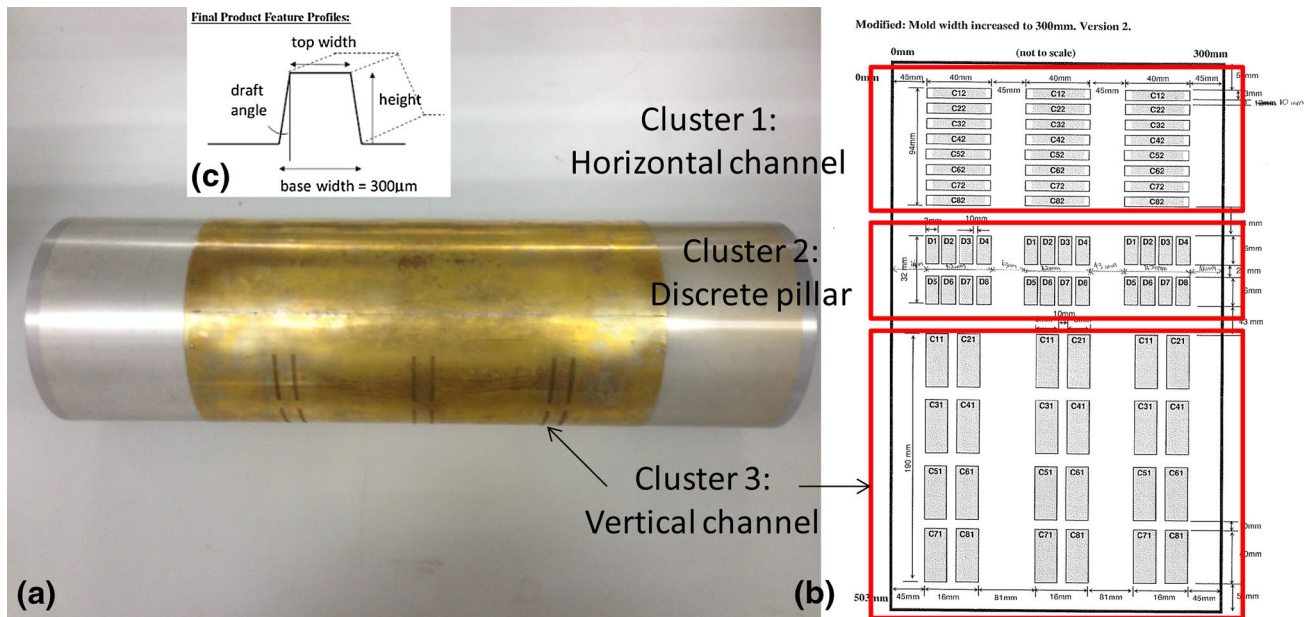
Fig. 2 **a** Image of the embossing roller mold; **b** layout of the brass sheet mold design; **c** an example of the micro feature design on the mold
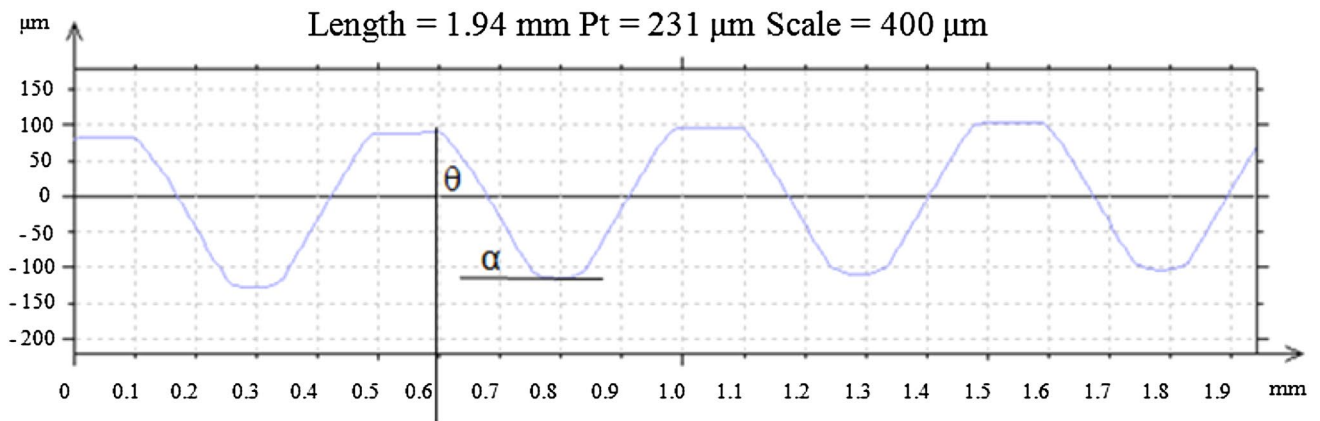

Fig. 3 3D optical microscope measurement result of brass mold surface features: $\Delta y = 210$; $\theta = 35°$

mold surface feature details is illustrated in Fig. 3. In addition, a temperature sensor is added to monitor the temperature changes during the UV embossing process.

The substrate, plainly called "backing film" or "film", is chosen to be HK-31 WF type of PET, which is lightweight, optically transparent and impact-resistant, ideal for UV embossing of large area optics applications. PET flexible film with a thickness of 125 μm is selected as the substrate in the current study with Young's modulus of 3GPa and tensile stress 200 MPa at 120 % elongation as measured by uniaxial tensile tests. Its surface was pretreated for promoting adhesion between the substrate and the UV curable resin.

The resin (Lentex_mix) in the current study is a special UV curable embossing lacquer mixed from Lentex_L™ and Lentex_50™, with advanced physical properties of optical transparency, heat resistance, high refractive index, high profile fidelity and antistatic. Its viscosity was measured using a rotational cylinder shear rheometer at different temperatures and shear rates. Figure 4 illustrates the base resins and the mix's behaviours under different shear rates. It can be observed that this type of resin is not sensitive to the shear rate, very similar to Newtonian fluid. Figure 5 illustrates the temperature dependency of the shear rate in the base and mix resins. A clear drop in the viscosity can be observed with increasing temperature. It is not a trivial
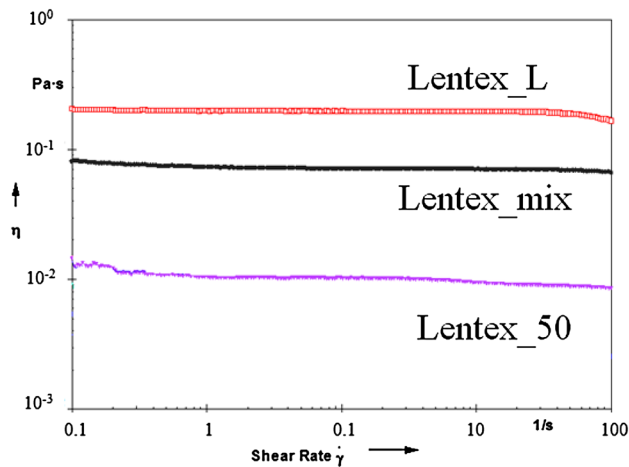
Fig. 4 Viscosities of the base resins and the mix under different shear rates
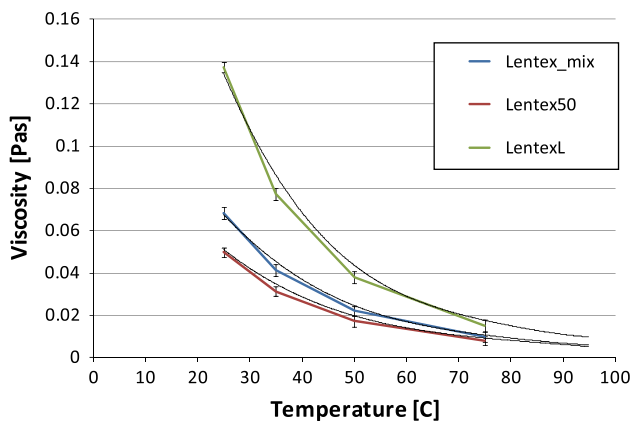
Fig. 5 Viscosities of the base resins and the mix under different temperatures

issue as the intensive UV lighting during the curing process will heat up the embossing roller significantly to 80° as measured by our temperature sensor and reduce the resin viscosity. Therefore, the current model needs to take this into consideration. A simple way to achieve this is to use one viscosity value at fixed temperature simulation runs. If room temperature is considered, the simulation will be more close to an "upper bound" estimation of the resin filling time; if 80 °C (at which the system runs stable) is considered, the simulation will be more close to the "lower bound" estimation of the resin filling time.

In all, some of the specifications and experimental parameters are summarized briefly as follows:

- Film web width: 500 mm (max).
- Film thickness: 125 μm
- Viscosity: ~0.01 Pa s @ 80 °C

- Web speed: max. 30 m/min
- Coating width: 250 mm
- Coating thickness: 200 μm
- Residual layer thickness: 50 μm

2.2 Numerical simulation based on Coupled Eulerian Lagrange (CEL) algorithm

Coupled Eulerian–Lagrangian (CEL) algorithm was introduced by ABAQUS™ from v6.8 onwards to allow analysis of both Eulerian and Lagrangian bodies within the same model to interact. Coupled Eulerian–Lagrangian analysis is typically used to model the interactions between a solid body and a yielding or fluid material, such as an Eulerian gas inflating a Lagrangian airbag. Such analyses can only be performed in explicit dynamic steps, and a powerful general contact definition was created to enable contact between Lagrangian and Eulerian parts as well as different Lagrangian parts. CEL algorithm is perfectly suitable for UV R2R embossing filling stage study as the film tension will affect the resin flow during filling, and the filling of the resin will exert force back on the film, which can potentially deform the film and change the resin flow path. Such Fluid Structure Interaction (FSI) with large rotation and deformation is the target process that CEL algorithm aims at.

The model setup replicates that of the experiment (Fig. 1, UV embossing module) with its dimension indicated in Fig. 6. The area of interest is selected to be only around the initial tangential contact point between the film and embossing roller as we perceive that filling of the resin only occurs (very) locally around that position. Figure 7 provides the setup of the simulation model. The embossing roller is considered to be analytical rigid as it is much harder than the backing film and the liquid resin, and its surface is assumed to be hydrophobic as we coat the nano release agent prior to the process. The backing film is considered to be Lagrangian elasto-plastic with element type
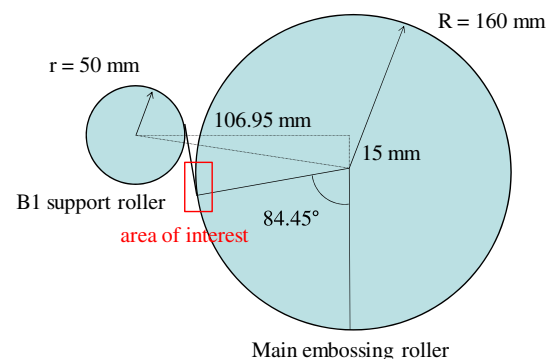
Fig. 6 Geometrical abstract of the UV embossing filling stage (not-to-scale)
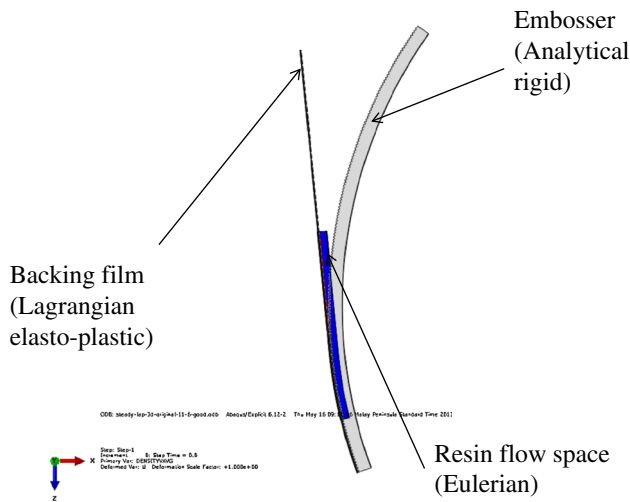
Fig. 7 Simulation model setup for the UV R2R embossing process

C3D8R and its surface to be fully hydrophilic due to the pre-treatment. Eulerian resin flow space with element type R3D4 was also created to account for the resin flow during the filling stage. Apart from viscosity (shear deformation), the Equation-of-State (EOS) of liquid resin has to be defined to account for the volumetric deformation that may occur during filling stage. Linear Us–Up Hugoniot form (Ahrens 1993) was adopted, with input of resin density $\rho = 1.05$ kg/l, speed of sound in resin v = 1400 m/s and the slope of the shock Hugoniot s, set to be zero for most of the liquid.

The initial conditions of the simulation were chosen to be those of the steady state of the backing film running into the embossing roller at constant speed with constant resin filling as this is the steady state of the production process and its feature geometry integrity is of great importance to the product quality. Constant angular and linear velocities

were prescribed at the beginning and end tips of the film respectively, and the pre-tension of the film was also considered in the initial step.

To speed up the simulation process, semi-automatic mass scaling and manual wave speed scaling were employed to increase the increment time. Kinetic energy was closely monitored throughout the process to ensure that it has minimal fluctuation.

3 Results and discussion

Figure 8 illustrates a time history of one resin filling cycle at web speed of 3 m/min. The color scale indicates the volume percentage of the resin in the Eulerian flow space. Red indicates 100 % volume occupancy (full resin filling) while blue means 0 % (no resin). Backing film and embossing roller only have their respective feature edges shown in the graph. The green cycle tracks the movement of one embossing roller "tooth" from the initial contact between the tooth and the resin at 0 s to the almost complete mold filling at 0.027 s. It can be seen that the filling stage is indeed a very quick process and only occurs very locally around the initial tangential contact point between the film and embossing roller. The assumption on the scope of the model setup is valid for the current study.

The mode of the embosser roller cavities filling is not exactly the same as the planar mold embossing, in which the mold moves perpendicular to the resin layer and press down. Here, the mold slides in at a small tangential angle at the same web speed as the backing film. In order to quantify such approaching angle, the resin filling distance has to be firstly defined. It is the web distance from the point where the "tooth" is in first contact with the resin to the point where the "root of the tooth" is in contact with the resin if a complete filling is achieved (The residual coating

Fig. 8 Time history of the resin filling at web speed of 3 m/min: **a** t = 0 s; **b** t = 0.005 s; **c** t = 0.018 s; **d** t = 0.027 s; *Green circle* tracks the movement of the same "tooth" on the embossing roller over one filling cycle
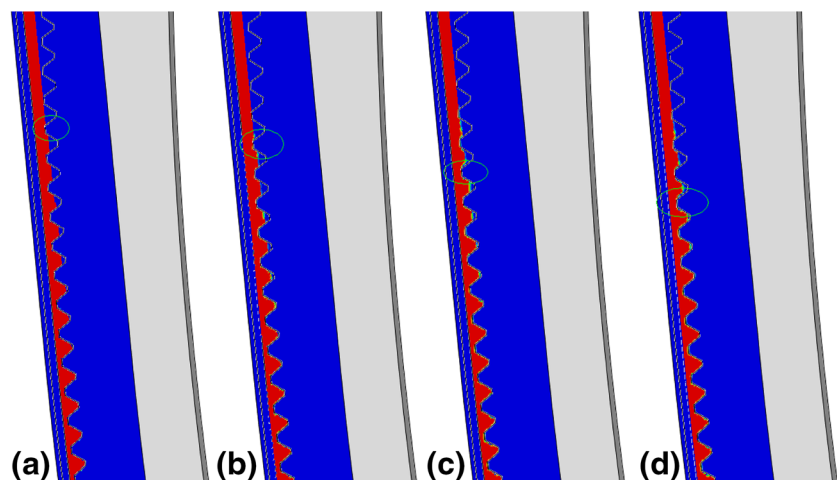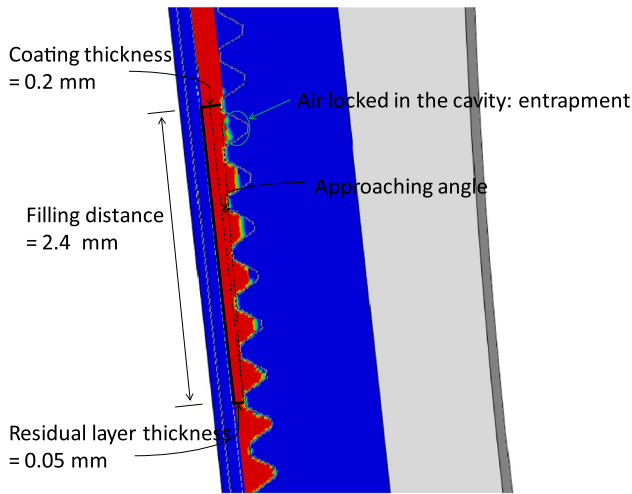
Fig. 9 A closer look at the filling stage at web speed of 3 m/min: the calculation of approaching angle and the phenomenon of air entrapment due to the setup geometry

thickness also becomes constant at this point). Therefore, the approaching angle can be approximated through a simple trigonometry illustrated in Fig. 9, which in our case is arctan ((0.2–0.05)/2.4) ≈ 3.58°. Bearing in mind that ~ 5° is considered a small angle in cosine Taylor expansion, therefore the mold filling in this R2R process still somehow looks similar to that of the planar mold filling.

It is indeed the case that the resin flows into the cavity in the simulation in an incremental way similar to planar mold filling. Figure 10 illustrates the time history of single cavity mold filling during R2R UV embossing, t = 0 s shows the start status of the simple cavity and t = 0.03 s indicates the end of the mold filling. The resin rises in the cavity in a level way, no significant sloshing or turbulence was found during the process. This may be due to the relative high viscosity and low web speed in the steady state of the current study. Such observation has two implications: (1) The mold cavity will have a complete filling in a short web travel distance if no air entrapment is considered, and (2) based on the setup geometry, the air entrapment is, unfortunately, unavoidable during filling (Fig. 9).

In order to study the UV R2R mold filling process under different conditions, some preliminary parametric studies have also been carried out. Figure 11a, b illustrate the filling distances of UV embossing with web speed of 3 m/min and 30 m/min respectively. It indicates that with 10× the speed, the filling distance only increase marginally from 2.4 mm to 2.8 mm. It is possibly caused by the resin backflow, and hence the slight flexing of the backing film. Such effect is minimal as it still achieves a complete fill. Therefore, we argue that the filling stage plays a minor role in the feature fidelity control if air entrapment is not considered. Should the filling stage contribute to the geometry fidelity loss, it would come from the air entrapment during the

Fig. 10 Time history of single cavity mold filling during R2R UV embossing at web speed of 3 m/min
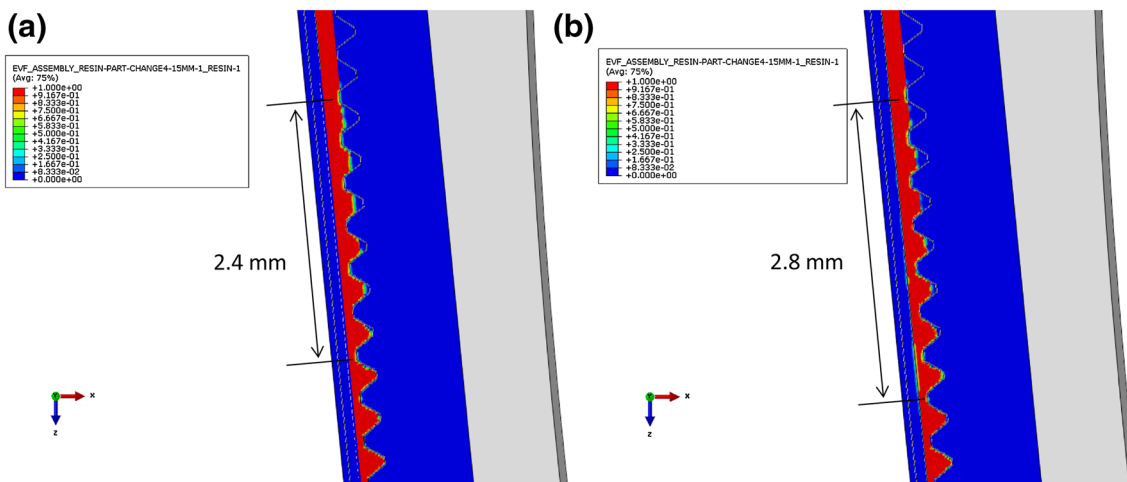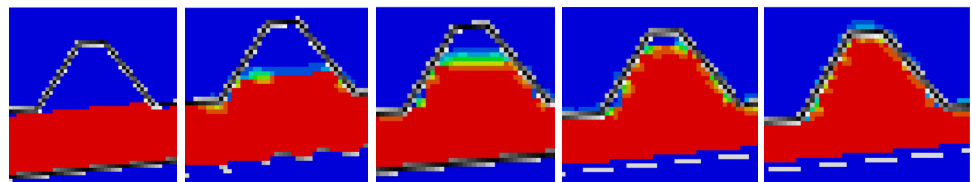
Fig. 11 Comparison of the filling distance between **a** v = 3 m/min and **b** v = 30 m/min simulation models
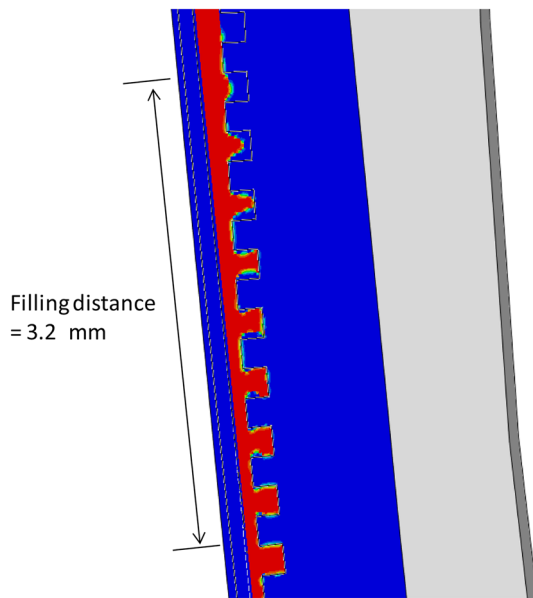
Fig. 12 A snapshot of the filling stage of R2R UV embossing at web speed of 3 m/min with embossing roller cavity feature of no tapering angle. Take note that the cavity is filled in the center and top first, then two side walls are filled later

filling of individual cavity, which was determined by the geometry of the setup. Therefore it can only be removed through external assistance (i.e. vacuum).

Study on the effect of the cavity tapering angle has also been carried out. Figure 12 illustrates the filling stage of a fictional R2R UV embossing process with 1° taping angle cavity at web speed of 3 m/min. It shows that a complete fill still can be achieved. The filling distance is about 3.2 mm, which is longer than previous 35° tapered cavity embosser. It can be expected that the smaller the tapering angle, the higher the web speed, the more difficult to fill the mold cavity. It is also interesting to note that the mode of filling is no longer level incremental, but with turbulence that the resin will reach the top of the cavity first then flow sideways and backwards to fill the remaining space near the side walls in the cavity as illustrated in Fig. 13.

As it is still hard to capture the time-lapse motion of the mold filling process in R2R [although limited success has been achieved on low speed planar embossing (Wang et al. 2012)], the experimental validation in the current study is still carried out by measuring the final feature dimensions, which is under the influence of both mold filling and

Fig. 13 Time history of single non-tapered cavity mold filling during R2R UV embossing at web speed of 3 m/min
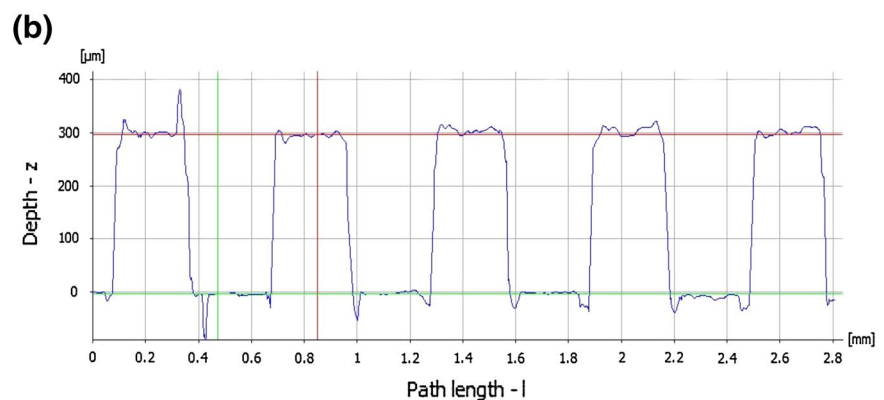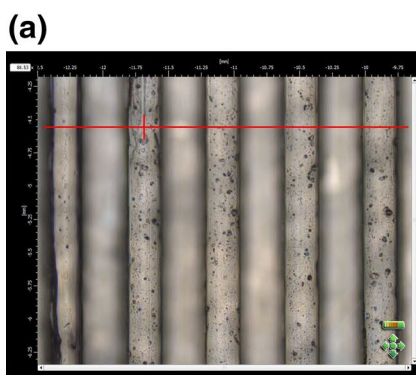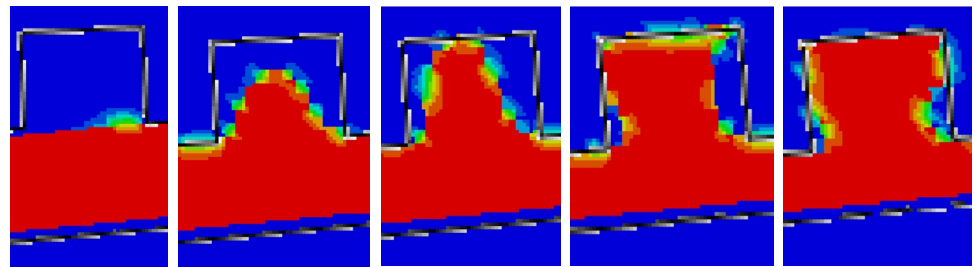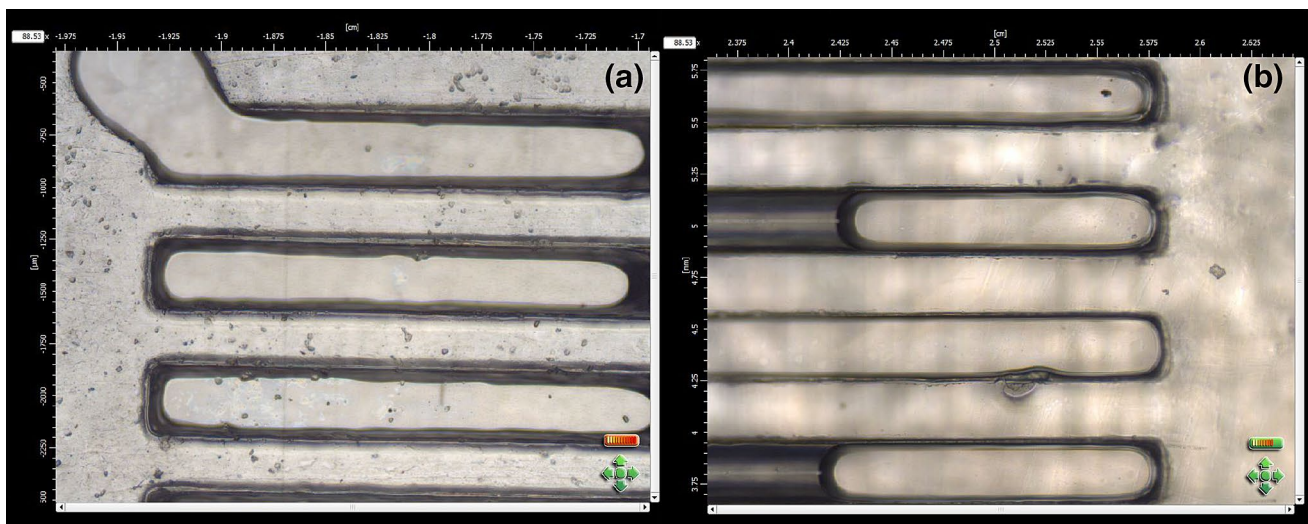

Fig. 14 3D optical micrograph of **a** the vertical continuous channel features and **b** their dimensions

demolding. However, the final feature surface may still be able to give some indication on the process details: if incomplete feature surfaces are smooth and glossy, it is likely caused by the air entrapment; and if incomplete feature surfaces contains sharp edges and dull, it may due to the brittle fracture during the demolding process (feature breaks). The extreme case of it will be peel-off of the entire feature, leaving only a hole on the residual layer.

Figure 14 illustrates an example of the complete filled vertical continuous channels with height of 300 μm. The height reaches the full mold cavity depth and there is no obvious defect or void present in the micro feature. In a matter of fact, most of the vertical channels including the

higher AR ones (AR = 1 and 1.5) are fully filled, representing no difficulty in mold filling and demolding. This success is geometrically determined: since the channel cavity is running along the rolling direction, there is no such "tooth" in front of or behind the rolling direction as in Fig. 9. Hence the air will not be locked in the cavity and there is always a vent for air passage. This geometrical determined concept also applies to demolding as there is also no "tooth" blockage in the rolling direction.

Figure 15 illustrates the (a) fully peel-off and (b) incomplete filling of the horizontal continuous channels. Such phenomenon is not unusual as only less than 10 % horizontal continuous channels have been fully filled in a 5 min
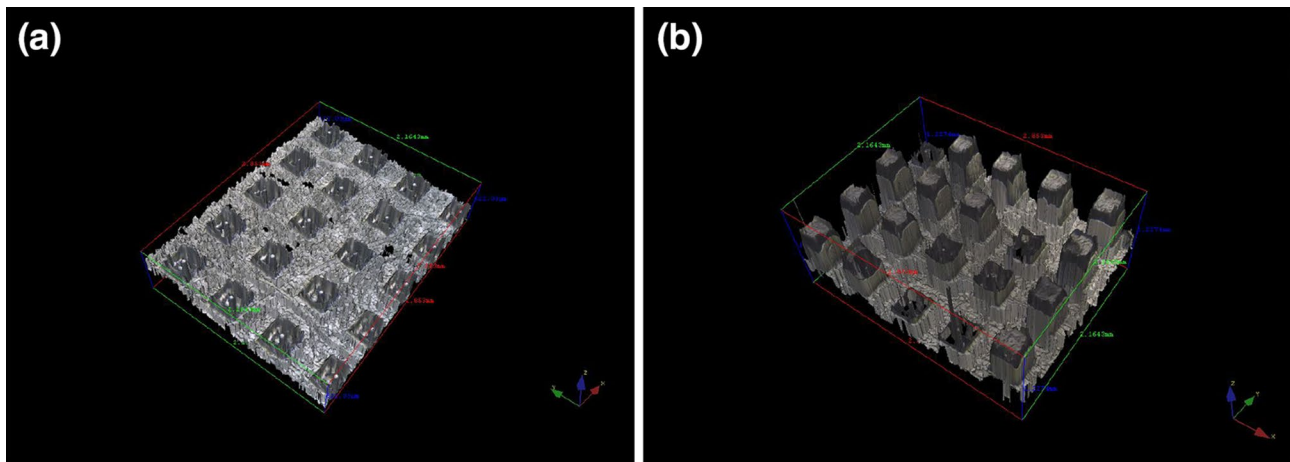

Fig. 15 3D optical micrograph of **a** fully peel-off and **b** incomplete filling of the horizontal continuous channels
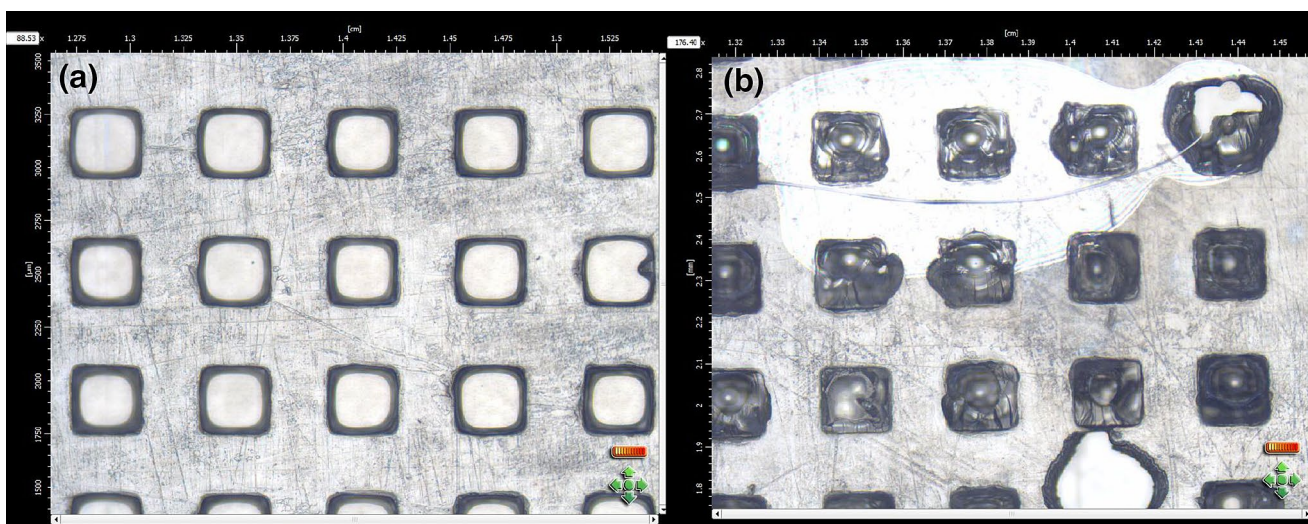
Fig. 16 3D optical micrograph of **a** fully and **b** partially peel-off of the discrete pillar features

Fig. 17 Image reconstruction in Alicona 3D Optical Metrology system for discrete pillar fabricated **a** without degassing and **b** with degassing

continuous test. This implies that the numerical model prediction is capable of capturing the fundamental features of the mold filling process where geometrically determined air entrapment (Fig. 9) plays a major role in the feature fidelity. One design rule we may derived from it is: if there is a continuous profile to be produced using the existing R2R UV embossing setup, it is better to make it along the rolling direction (vertical) rather than perpendicular to it (horizontal).

For the case of discrete pillars, Fig. 16 illustrates the partial or complete peel-off of the discrete pillar in the residual layer. No single pillar was formed successfully after the test. A planar embossing using the same pillar dimensions further confirm the effect of the air entrapment: As shown in Fig. 17, the resin was unable to fill the mould to the cavity height and hence, only partial features were replicated. This is still too high for the R2R embossing process, as it will still stick to the rotating mold and peel-off the residual layer. However, with degassing, the resin was able to fill the mould and replicate the full feature in the planar embossing. However, in the R2R process, it will be peeled off as well due to geometrical constraint.

4 Conclusions

In this work, the filling stage of the R2R UV embossing process has been studied through numerical simulation and experimental validation. Coupled Eulerian Lagrange (CEL) algorithm was employed to consider both the deformation of the solid (backing film) and the flow of the liquid (UV resin). Models predict that under current circumstances, complete filling of the cavities can be achieved if air entrapment is not taken into consideration. However, the geometry of the setup indicates there will

be air pockets locked in the cavity during the filling of the resin. For the web speed of 3 m/min and 30 m/min, the filling distance for the tapered cavity with angle of 35° increases fractionally from 2.4 mm to 2.8 mm. For filling cavities without taper, the filling distance is 3.2 mm, which is longer than that of the tapered one at the same web speed.

References

Ahn SH, Guo LJ (2008) High-speed roll-to-roll nanoimprint lithography on flexible plastic substrates. Adv Mater 20:2044–2049

Ahn SH, Guo LJ (2009) Large-area roll-to-roll and roll-to-plate nanoimprint lithography: a step toward high- throughput application of continuous nanoimprinting. ACS Nano 3:2304–2310

Ahrens TJ (1993) Equation of state. High pressure shock compression of solids, Springer, New York

Becker H, Heim U (2000) Hot embossing as a method for the fabrication of polymer high aspect ratio structures. Sensor Actuat A-Phys 83:130–135

Guo LJ (2004) Recent progress in nanoimprint technology and its applications. J Phys D Appl Phys 37:R123–R141

He Y, Fu JZ, Chen Z (2007) Research on optimization of the hot embossing process. J Micromech Microeng 17:2420–2425

Lee HS (2007) UV nano embossing for polymer nano structures with non-transparent mold insert. Microsyst Technol 13:593–599

Li JM, Liu C, Qiao HC, Zhu LY, Chen G, Dai XD (2008) Hot embossing/bonding of a poly (ethylene terephthalate) (PET) microfluidic chip. J Micromech Microeng 18:015008

Makela T (2008) Continuous double-sided roll-to-roll imprinting of polymer film. Jpn J Appl Phys 47:5142–5144

Nezuka O, Yao D, Kim BH (2008) Replication of microstructures by roll-to-roll UV-curing embossing. Polym-Plast Technol 47:865–873

Sahli M, Khan MC, Gelin JC (2009) 3D modelling and simulation of the filling of cavities by viscoelastic polymer in roll embossing process. Int J Mater Form 2(Suppl 1):725–728

Sahli M, Gelin JC, Barrière T (2010) Numerical modelling of the polymers replicatioin in micro-cavities by the roll embossing process. Int J Mater Form 3(Suppl 1):607–610

Schift H (2008) Nanoimprint lithography: an old story in modern times? A review. J Vac Sci Technol, B 26:458–480

Shan XC, Chua KM, Soh YC, Lu CW (2009) Determining the optimal process conditions of micro roller embossing for large-area patterning of green ceramic substrates. J Micromech Microeng 19:017001

Shan XC, Lau SK, Mohahidin MB, Liu T, Lu CW (2011) Formation of large format functional films via roll-to-roll (R2R) ultraviolet (UV) embossing. In: Proceeding of IEEE 13th electronics packaging technology conference, 07–09 Dec, Singapore, E-ISBN 978-1-4577-1981-3, 521–524

Wang Q, Hiroshima H, Suzuhi K, Youn SW (2012) Real-time full-area monitoring of the filling process in molds for UV nanoimprint lithography using dark field illumination. J Vac Sci Technol B 30(6):06FB13–06FB13-6

Worgull M, Heckele M (2004) New aspects of simulation in hot embossing. Microsyst Technol 10:432–437

Worgull M, Hetu JF, Kabanemi K, Heckele M (2006) Modeling and optimization of the hot embossing process for micro- and nano-component fabrication. Microsyst Technol 12:947–952

Yeo LP, Joshi SC, Lam YC, Chan-Park MB, Hardt DE (2009) Numerical analyses of peel demolding for UV embossing of high aspect ratio micro-patterning. Microsyst Technol 15:581–593

Yeo LP, Ng SH, Wang ZF, Xia HM, Wang ZP, Thang VS, Zhong ZW, de Rooij N (2010) Investigation of hot roller embossing for microfluidic devices. J Micromech Microeng 20:015017